

## Supporting Information for

### **Bio-inspired design of an *in-situ* multifunctional polymeric solid-electrolyte interphase for Zn metal anode cycling at 30 mA cm<sup>-2</sup> and 30 mA h cm<sup>-2</sup>**

Xiaohui Zeng<sup>a</sup>, Kaixuan Xie<sup>b</sup>, Sailin Liu<sup>a</sup>, Shilin Zhang<sup>ac</sup>, Junnan Hao<sup>c</sup>, Jiayu Liu<sup>d</sup>, Wei Kong Pang<sup>a</sup>, Jianwen Liu<sup>e</sup>, Pinhua Rao<sup>f</sup>, Qinghong Wang<sup>\*b</sup>, Jianfeng Mao<sup>\*ac</sup>, Zaiping Guo<sup>\*ac</sup>

<sup>a</sup> Institute for Superconducting and Electronic Materials (ISEM), Australian Institute for Innovative Materials (AIIM), University of Wollongong, NSW 2522, Australia.

<sup>b</sup> School of Chemistry and Materials Science, Jiangsu Normal University, Xuzhou, Jiangsu 221116, P. R. China.

<sup>c</sup> School of Chemical Engineering & Advanced Materials, University of Adelaide, Adelaide, SA 5005, Australia.

<sup>d</sup> School of Mechanical and Manufacturing Engineering, University of New South Wales, Sydney, NSW 2052, Australia.

<sup>e</sup> College of Chemistry and Chemical Engineering, Hubei University, Wuhan 430062, P. R. China.

<sup>f</sup> College of Chemistry and Chemical Engineering, Shanghai University of Engineering Science, Shanghai 201620, P. R. China.

## 1. Experimental section

**Preparation of electrolytes and electrodes.** Zinc triflate ( $\text{Zn}(\text{CF}_3\text{SO}_3)_2$ ), zinc sulfate ( $\text{ZnSO}_4 \cdot 7\text{H}_2\text{O}$ ), dopamine (DA) hydrochloride, and divanadium pentoxide ( $\text{V}_2\text{O}_5$ ) were purchased from Sigma Aldrich. Zn foil (10 and 60  $\mu\text{m}$ , 99.9 %), Ti foil (30  $\mu\text{m}$ , 99.9 %), Cu foil, glass fibre (0.96 mm), and mixed cellulose membrane (30  $\mu\text{m}$ ) were purchased from Shenzhen Kejing Star Technology. The blank electrolytes were prepared by dissolving 1 M  $\text{Zn}(\text{CF}_3\text{SO}_3)_2$  and 1 M  $\text{ZnSO}_4$  in deionized water, respectively. The electrolytes with different concentrations of DA (i.e., 5, 25, 50, and 100 mM) were prepared by adding a certain amount of DA into the blank electrolytes and sealing them well for use. The  $\text{V}_2\text{O}_5$  electrodes were prepared by a slurry coating method on Ti foil, where commercial  $\text{V}_2\text{O}_5$  powder, Super P, and polyvinylidene fluoride (PVDF) in a mass ratio of 7:2:1 were mixed in N-methyl-2-pyrrolidone (NMP). The active loading masses for the  $\text{V}_2\text{O}_5$  electrodes were about 4.8  $\text{mg cm}^{-2}$  (1.39 mA h  $\text{cm}^{-2}$ ) and 9.6  $\text{mg cm}^{-2}$  (2.8 mA h  $\text{cm}^{-2}$ ). Zn foil was punched into discs, which were directly used as Zn electrodes. Ultrathin Zn electrodes (10  $\mu\text{m}$ , 5.85 mA h  $\text{cm}^{-2}$ ) were used for the full cell tests. The amount of electrolyte used in the symmetric Zn/Zn and asymmetrical Zn/Cu cells was controlled at 100  $\mu\text{L}$ .

**Characterization.** The morphologies of the electrodes were characterized by field emission scanning electron microscopy (FESEM, JEOL JSM-7500FA) along with energy dispersive X-ray spectroscopy (EDX) mapping. *In-situ* Raman spectroscopy (JY HR800 Spectrometer) was conducted on a sealed cell (ECC-Opto-Std) with an optical window. The laser light was focused onto the sample using a 100 $\times$  objective with a long working distance. The laser power was 1 mW, and the accumulation time for each spectrum was set at about 10 s to avoid laser induced degradation. Atomic force microscopy (AFM) images were acquired in tapping mode using a Cypher ES AFM (Asylum Research, US). The specimen of cycled Zn electrode for cryogenic

electron microscopy (cryo-EM) was prepared by focused ion beam (FIB) milling on a FEI Helios Nanolab with a Ga<sup>+</sup> ion beam. The surface of the specimen was coated with a Pt/C protective layer. Cryo-EM images were acquired on a JEOL JEM-ARM200F at liquid N<sub>2</sub> temperature to eliminate contamination and reduce beam damage to the SEI layer. X-ray photoelectron spectroscopy (XPS) testing was performed on an X-ray photoelectron spectrometer (Thermo Fisher K-Alpha system). The XPS depth profiles were acquired by applying an Ar<sup>+</sup> beam with a scanning region of 200 × 200 μm and a sputtering rate of 2 kV. Fourier transform infrared (FTIR) mapping was performed on a Bruker Vertex 80v spectrometer coupled with a Hyperion 3000 FT-IR microscope. *In-situ* observations of Zn plating were carried out using an ECC-Opto-Std test cell.

***Electrochemical testing.*** The electrochemical performance of the batteries in this work was evaluated by using CR2032 coin-type cells on a Land BT2000 battery test system. The Zn plating/stripping tests were performed on Zn symmetrical cells in the electrolytes with and without DA. Coulombic efficiency (CE) measurements were carried out on asymmetrical Zn/Cu cells. Linear polarization analyses were conducted using a three-electrode device with Zn foil (working electrode), Ag/AgCl (reference electrode), and Pt (counter electrode). Electrochemical impedance spectroscopy (EIS) was implemented using a Biologic VMP-3 electrochemical workstation within the range of 10<sup>5</sup> to 10<sup>-2</sup> Hz. The Zn/V<sub>2</sub>O<sub>5</sub> cells were cycled between 0.2 and 1.6 V vs. Zn/Zn<sup>2+</sup>, and the specific capacities were evaluated according to the active mass of V<sub>2</sub>O<sub>5</sub>. Hydrophilic mixed cellulose membranes were applied as the separator in Zn/V<sub>2</sub>O<sub>5</sub> full cells with controlled electrolyte volume. Cyclic voltammetry (CV) of the Zn/V<sub>2</sub>O<sub>5</sub> cells was carried out on a Biologic VMP-3 electrochemical workstation.

***Calculation methods.*** The first-principles density functional theory (DFT) calculations in this work were conducted by using the Vienna Ab initio Simulation Package (VASP) with the

projector augmented wave (PAW) method<sup>1,2</sup>. The generalized gradient approximation (GGA) with the Perdew-Burke-Ernzerhof (PBE) functional was used to describe the exchange-correlation interaction<sup>3</sup>. The energy cut-off was set at 450 eV. For geometry relaxation, the convergence criterion was set at 0.03 eV/Å for force, and 10<sup>-4</sup> eV for energy. The Brillouin-zone integration was sampled by the single  $\Gamma$  point. The DFT-D3 mode was employed to simulate the van der Waals interaction<sup>4</sup>. Transition state searching was performed using the climbing-image nudged elastic band (CI-NEB) method<sup>5</sup>. The adsorption energy was calculated according to

$$E_{ads} = E_{total} - E_{Poly} - E_{Zn}$$

where  $E_{total}$  is the total energy of the Zn adsorbed system, and  $E_{Poly}$  and  $E_{Zn}$  are the energies of the PDA structure and the adsorption of a Zn atom, respectively.

## 2. Figures and tables

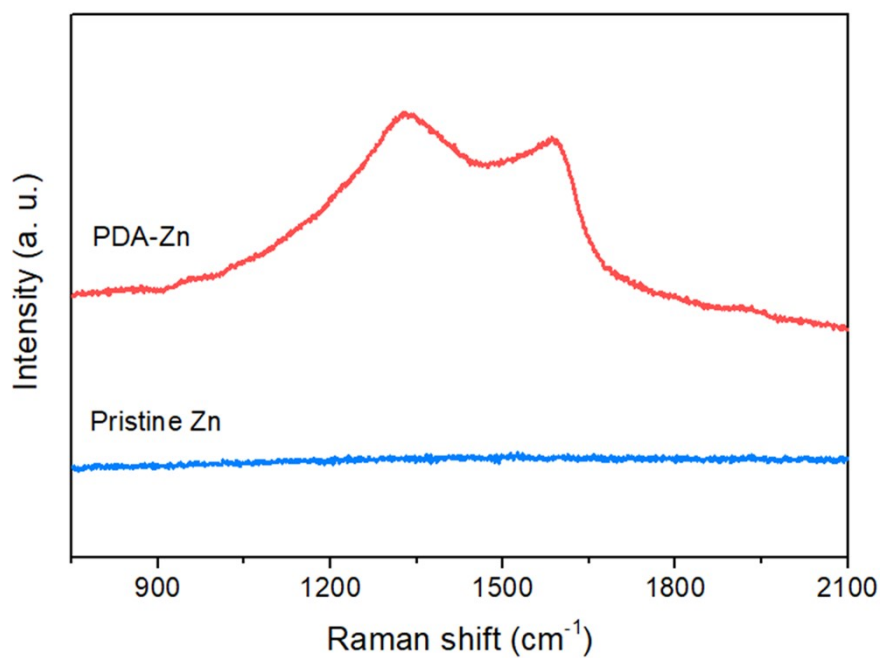


**Fig. S1** Raman spectra of pristine Zn and the *in-situ* PDA-Zn electrode. The Raman spectrum of PDA-Zn shows the typical stretching and deformation peaks of aromatic rings. The PDA-Zn electrode was stripped out of its symmetrical cell (1 mA cm<sup>-2</sup>, 1 mA h cm<sup>-2</sup>) after 10 cycles in the electrolyte (1 M Zn(CF<sub>3</sub>SO<sub>3</sub>)<sub>2</sub>) with DA.

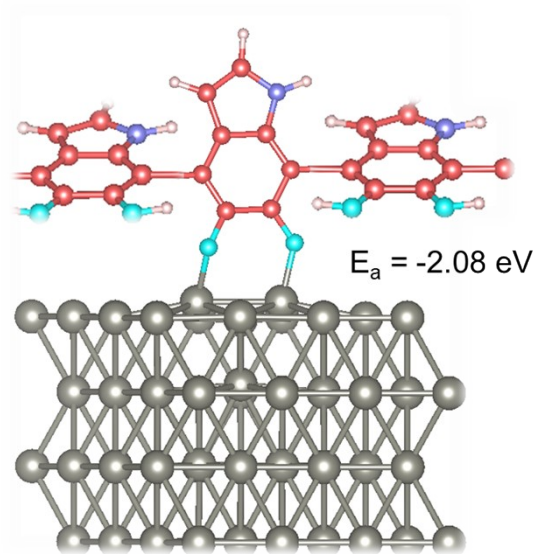


**Fig. S2** Geometrical configuration and adsorption energy of polydopamine (PDA) on the Zn (002) plane.

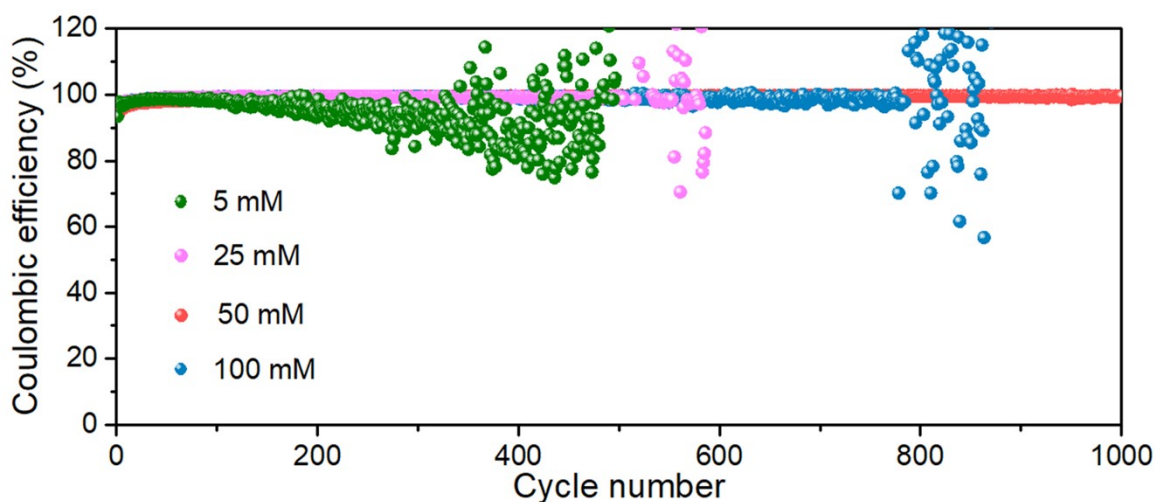


**Fig. S3** Comparison of the Coulombic efficiency of Zn plating/stripping on Cu in electrolytes consisting of 1 M  $\text{Zn}(\text{CF}_3\text{SO}_3)_2$  with different DA concentrations. The applied current density was  $1 \text{ mA cm}^{-2}$ , and the areal capacity was  $1 \text{ mA h cm}^{-2}$ . The Coulombic efficiency of Zn plating/stripping in electrolytes with a molarity of 50 mM DA additive shows the optimal electrochemical performance. When the concentration of DA additive in the electrolyte is too low, the PDA layer formed on Cu foil will be scattered and loose. This imperfect PDA layer is unable to suppress dendrite formation and parasitic reactions at the electrode/electrolyte interface, and consequently leads to unsatisfactory Coulombic efficiency of Zn plating/stripping on Cu. On the other hand, with excessive DA additive in the electrolyte, this polymeric layer would be very thick and not favorable for the ion-transfer kinetics during Zn plating/stripping processes.

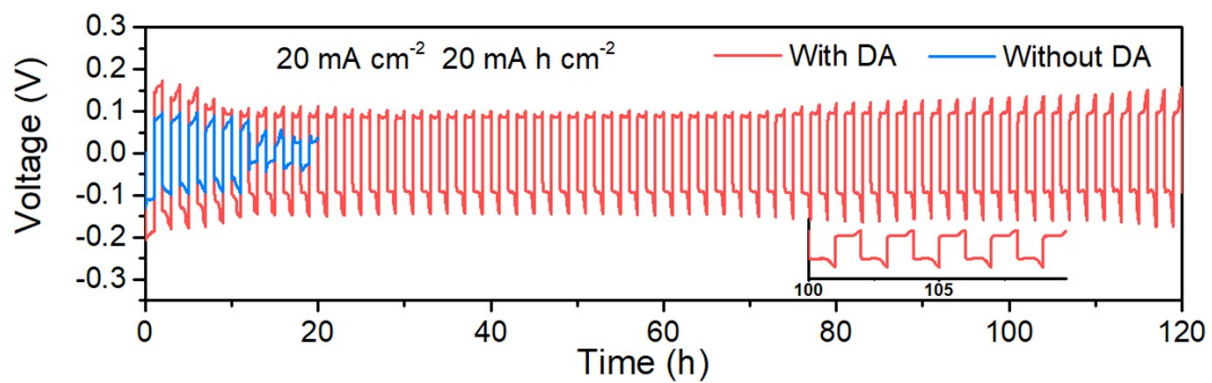


**Fig. S4** Comparison of the galvanostatic cycling properties of Zn symmetrical cells in the electrolytes with and without DA at  $20 \text{ mA cm}^{-2}$ ,  $20 \text{ mA h cm}^{-2}$ .

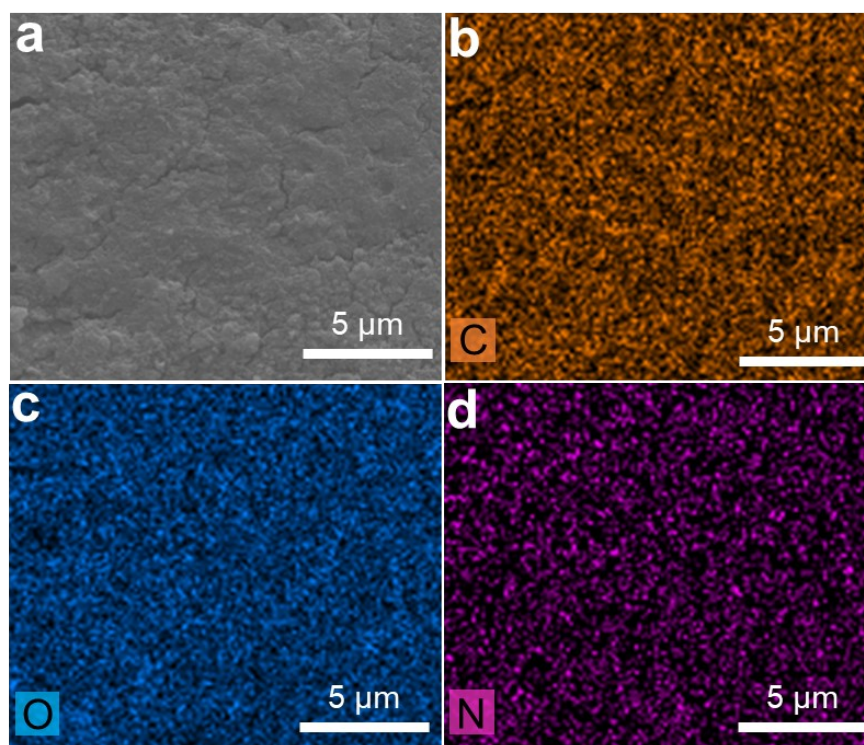


**Fig. S5** (a) Top-view SEM image and (b-d) corresponding EDX mapping of the Zn electrode after 10 cycles in the electrolyte with DA.

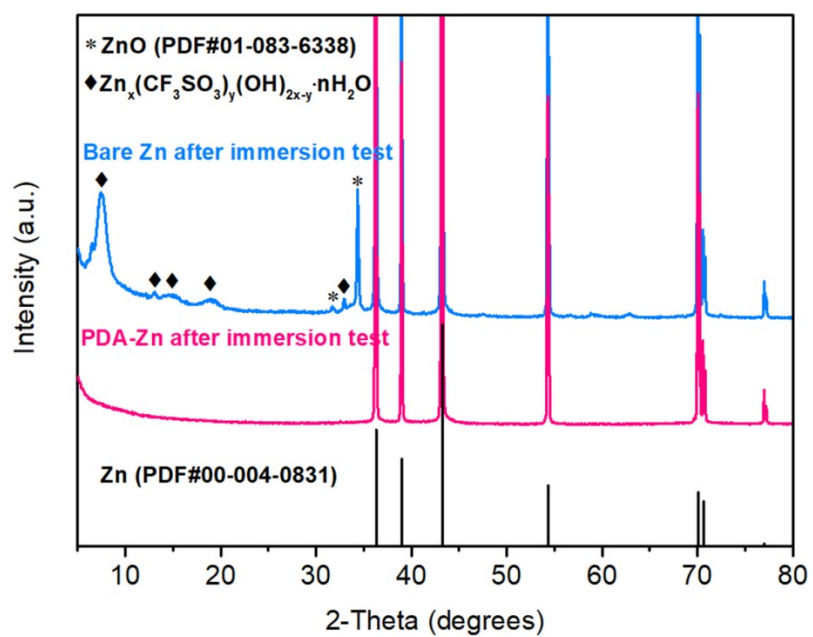


**Fig. S6** XRD patterns of bare Zn electrode and PDA-Zn electrode after immersion in aqueous electrolyte for 3 days.

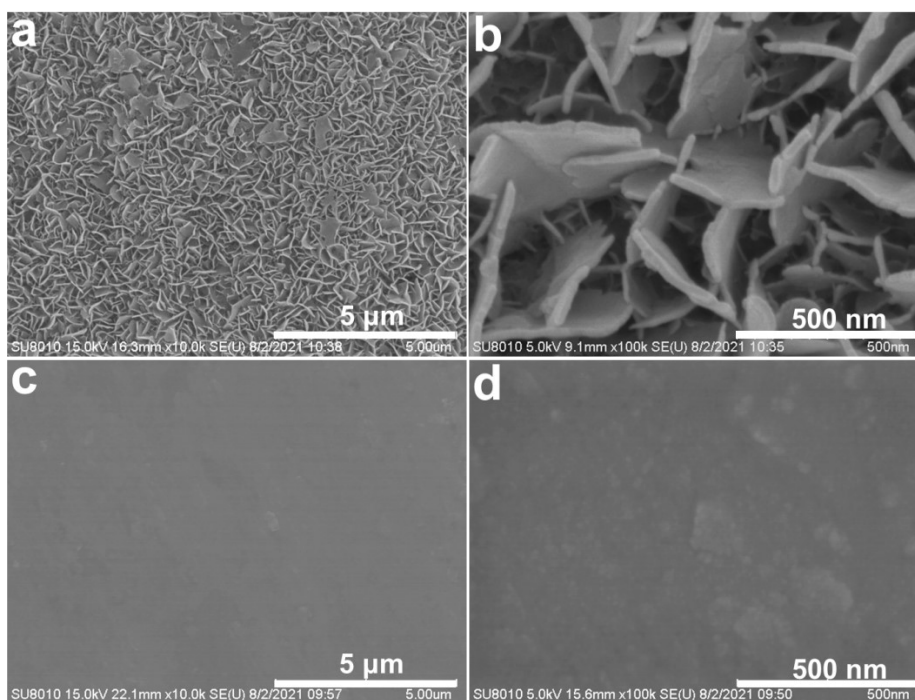


**Fig. S7** SEM images of (a, b) bare Zn electrode and (c, d) PDA-Zn electrode after immersion in aqueous electrolyte.

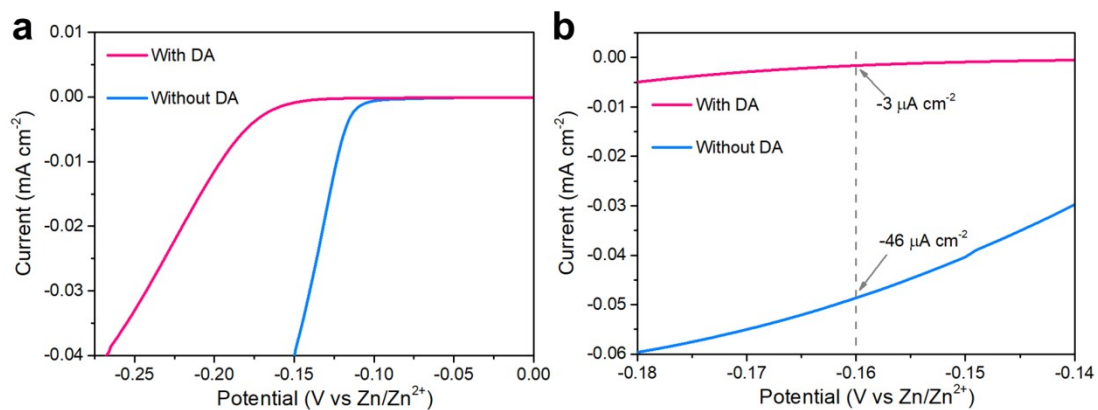


**Fig. S8** Linear sweep voltammograms (LSVs) of 1 M Zn ( $\text{CF}_3\text{SO}_3$ )<sub>2</sub> electrolyte with and without DA additive measured in a Zn/Ti half-cell at  $0.1 \text{ mV s}^{-1}$ .

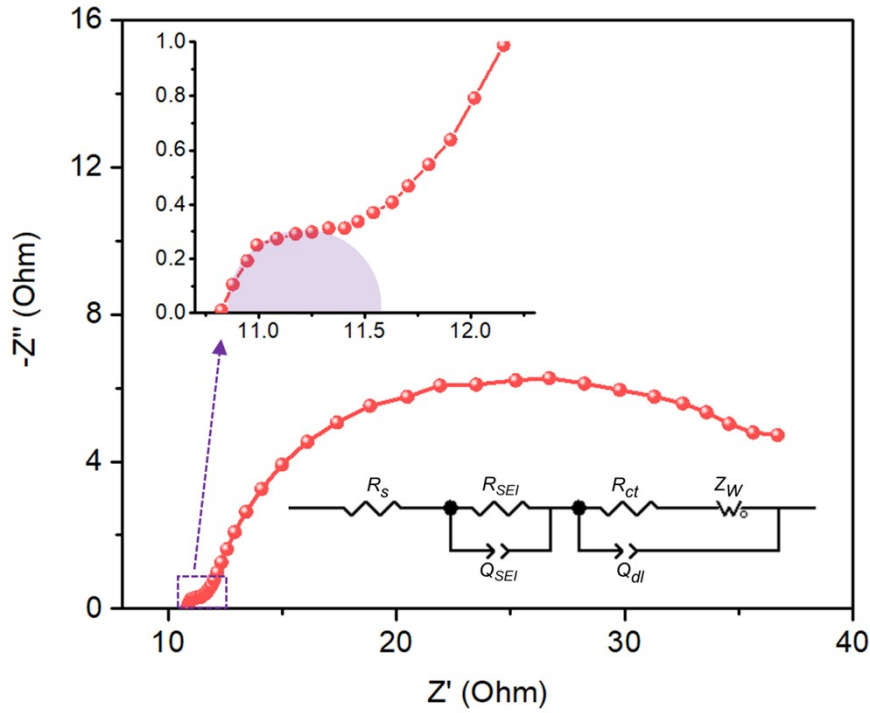


**Fig. S9** Fitted EIS spectrum of the PDA-Zn symmetrical cell. The upper inset is an enlargement of the indicated range, and the lower inset is the equivalent circuit.

The impedance spectrum of the PDA-Zn was collected at 25 °C over the frequency range from 1 MHz to 10 mHz. To determine the ionic conductivity of the PDA layer, the plot was fitted according to the equivalent circuit in the inset, where  $R_s$  reflects the resistance of the electrolyte,  $R_{SEI}$  represents the resistance of the interphase layer on the surface of the electrode, and  $R_{ct}$  represents the charge transfer resistance. The fitted value of  $R_{SEI}$  was 0.74  $\Omega$ , as shown in the enlargement of the indicated range. The ionic conductivity of PDA can be estimated based on the following equation:

$$\sigma = \frac{L}{R_b \cdot S}$$

where  $R_b$  is the resistance (0.74  $\Omega$ , as fitted),  $S$  is the area (0.5 cm<sup>2</sup> in this work), and  $L$  is the thickness of the PDA layer (40 nm in this work). Therefore, the ionic conductivity of PDA was evaluated as  $\sigma = 1.1 \times 10^{-5}$  S cm<sup>-1</sup>.

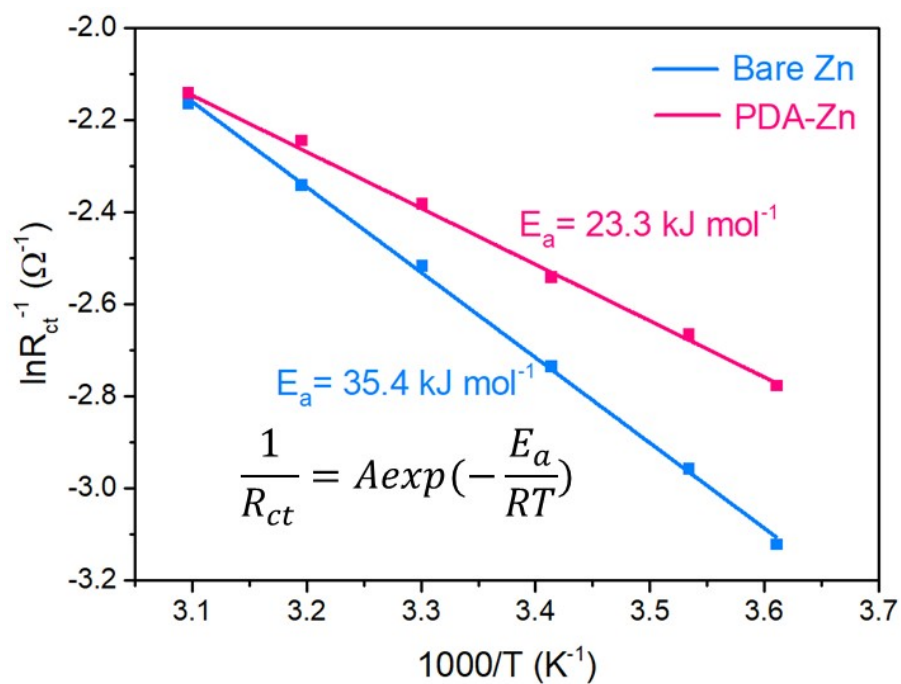


**Fig. S10** Arrhenius curves and activation energies of bare Zn and PDA-Zn, determined by EIS of symmetric cells at different temperatures. The symmetric cells were cycled for 20 cycles in the electrolyte with or without DA additive at room temperature.

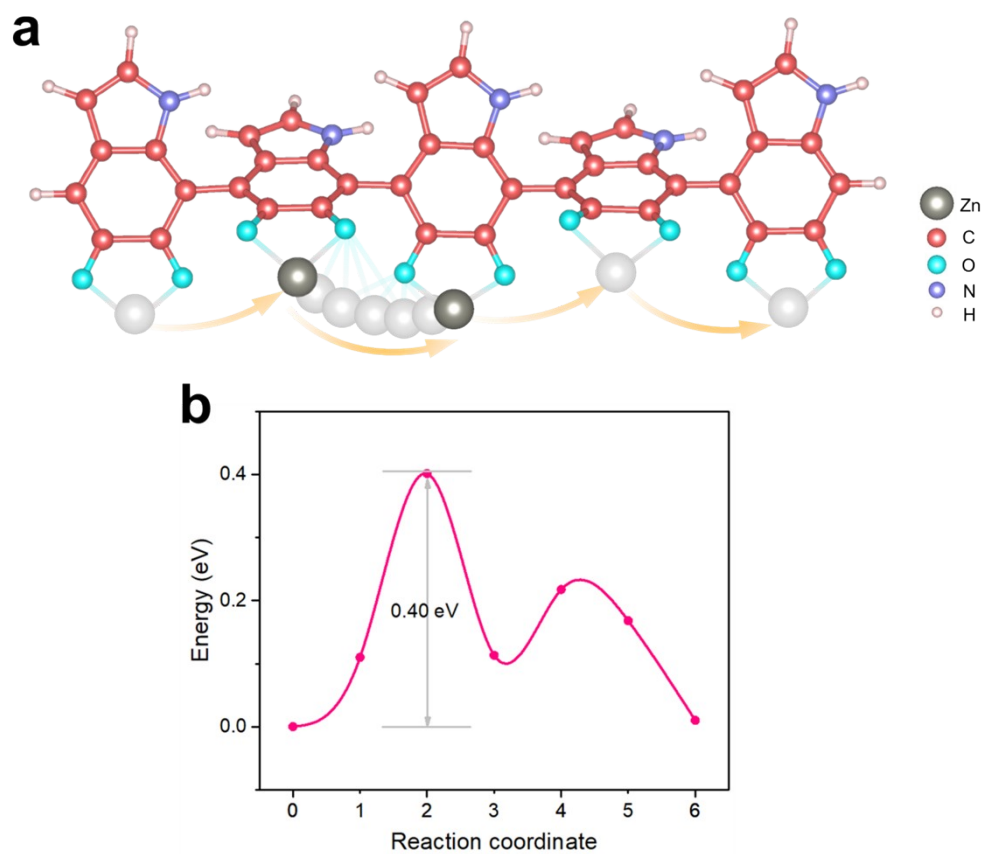


**Fig. S11** First-principles calculations of (a) the Zn-ion migration path in the PDA SEI layer and (b) the corresponding migration energy barrier.

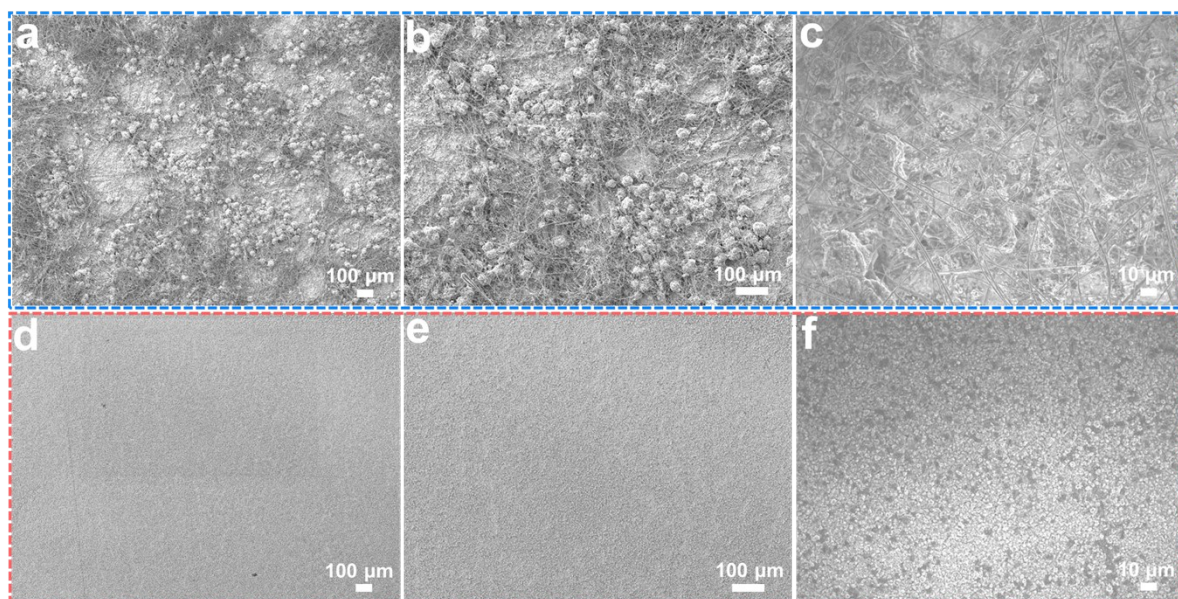


**Fig. S12** SEM images of Zn deposition morphology on Cu foil. (a-c) 1 M  $\text{Zn}(\text{CF}_3\text{SO}_3)_2$ , (d-f) 1 M  $\text{Zn}(\text{CF}_3\text{SO}_3)_2$  with DA as electrolyte. The applied current density was  $1 \text{ mA cm}^{-2}$ , and the areal capacity was  $1 \text{ mA h cm}^{-2}$ . The Cu foil was pre-cycled in Cu/Zn cells with the respective electrolytes for 5 cycles.

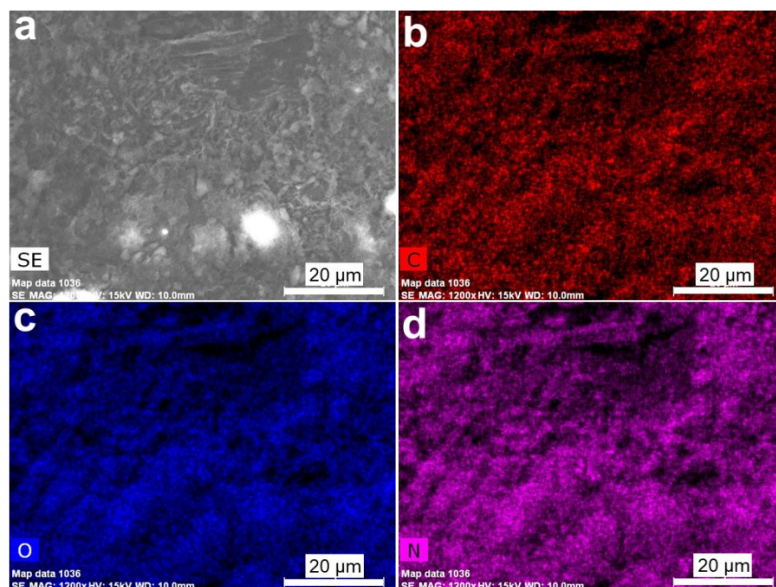


**Fig. S13** (a) SEM image and (b-d) corresponding EDX mapping of the Zn electrode after 400 h of plating/stripping in electrolyte with DA.

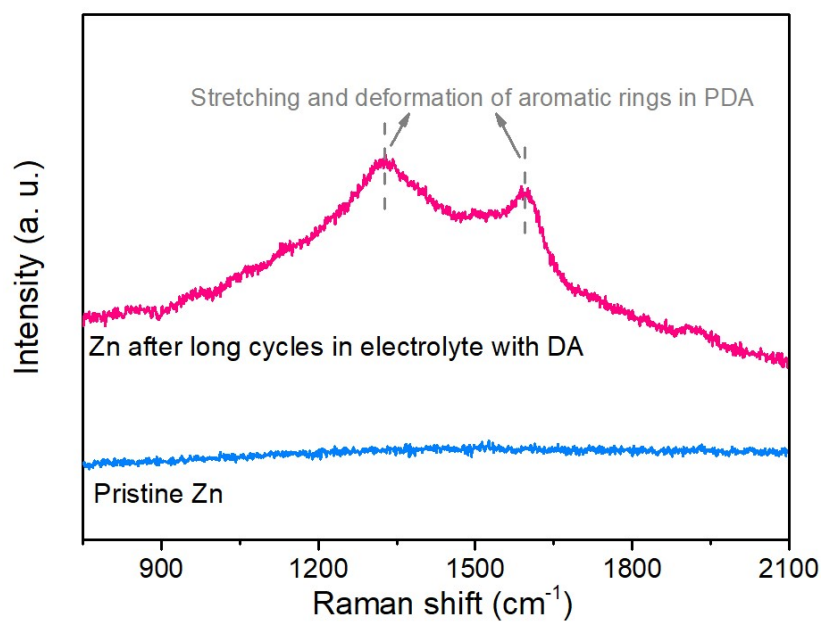


**Fig. S14** Raman spectra of pristine Zn and Zn electrode after long cycling in electrolyte with DA. The cycled Zn electrode was stripped out of its symmetrical cell ( $1 \text{ mA cm}^{-2}$ ,  $1 \text{ mA h cm}^{-2}$ ) after 400 h of plating/stripping in electrolyte with DA. The Raman spectrum of long-cycled Zn still shows the typical stretching and deformation peaks of aromatic rings in PDA.

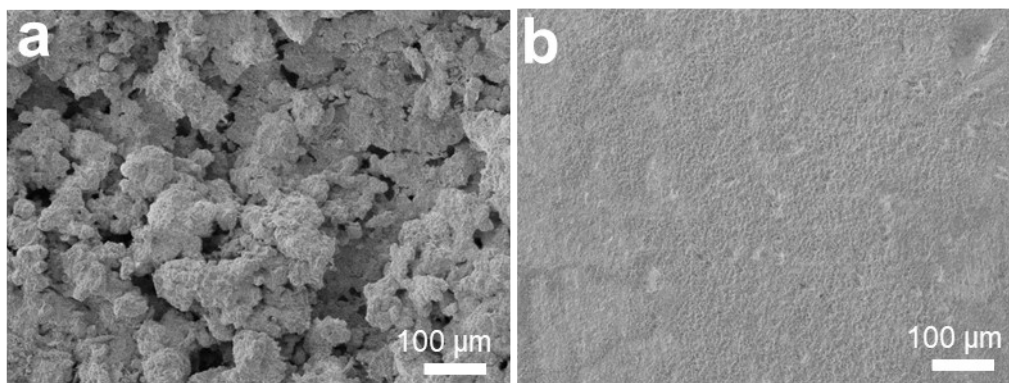


**Fig. S15** Top-view SEM images of Zn electrodes after 400 h of plating/stripping. (a) 1 M  $\text{Zn}(\text{CF}_3\text{SO}_3)_2$ , (b) 1 M  $\text{Zn}(\text{CF}_3\text{SO}_3)_2$  with DA as electrolyte.

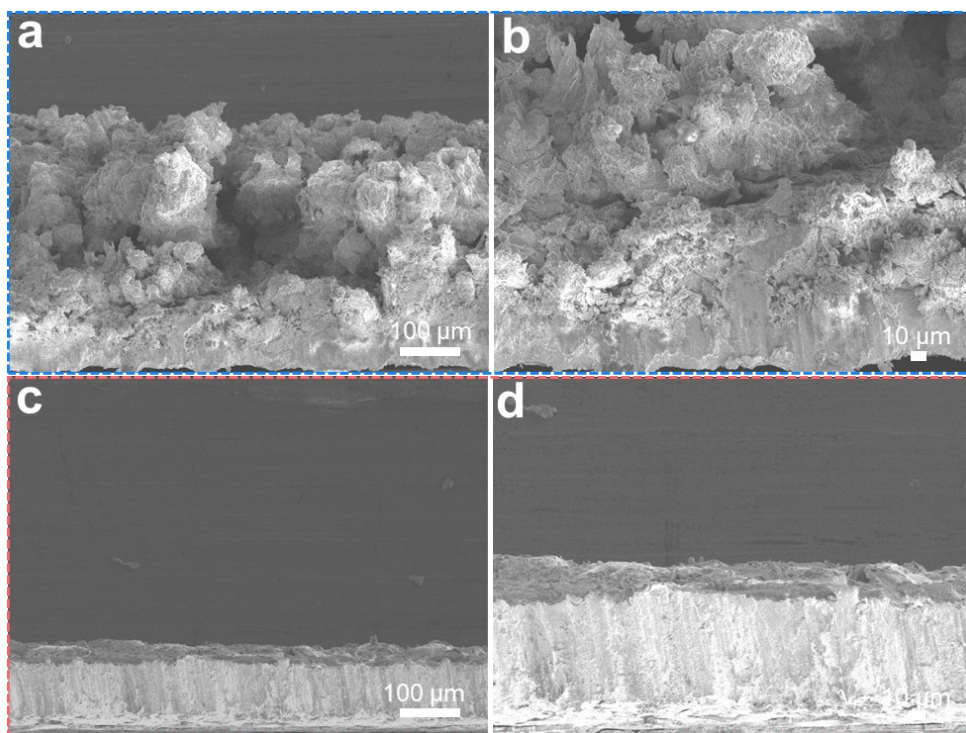


**Fig. S16** Side-view SEM images of Zn electrodes after 400 h of plating/stripping. (a, b) 1 M  $\text{Zn}(\text{CF}_3\text{SO}_3)_2$ , (c, d) 1 M  $\text{Zn}(\text{CF}_3\text{SO}_3)_2$  with DA as electrolyte.

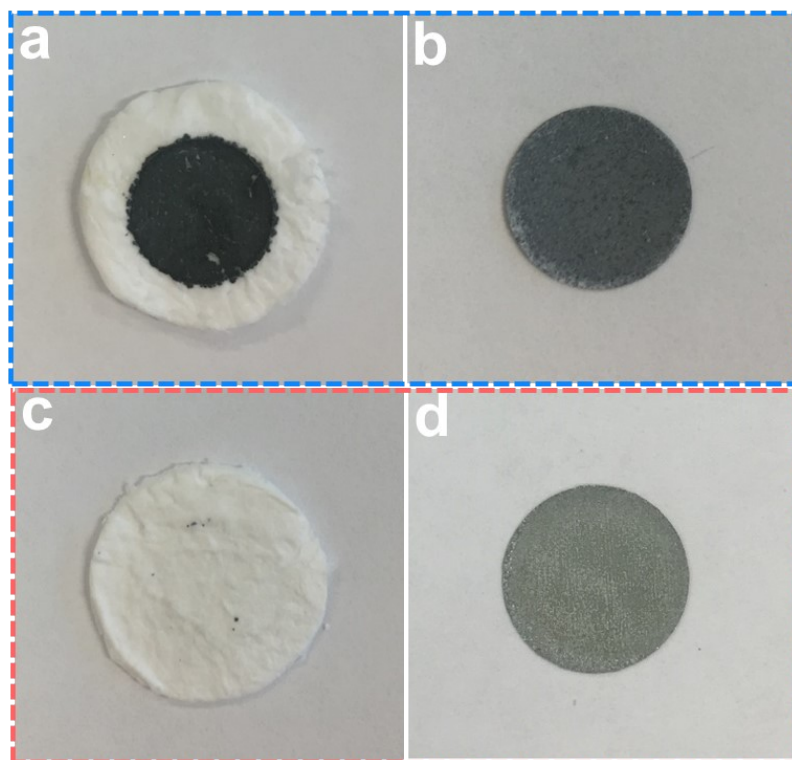


**Fig. S17** Digital images of Zn electrodes and glass fiber separators stripped from symmetrical cells after 400 h. (a) Glass fiber separator and (b) Zn electrode after cycling in the 1 M  $\text{Zn}(\text{CF}_3\text{SO}_3)_2$  electrolyte. (c) Glass fiber separator and (d) Zn electrode after cycling in the electrolyte with DA. The applied current density was  $1 \text{ mA cm}^{-2}$ , and the areal capacity was  $1 \text{ mA h cm}^{-2}$ . In 1 M  $\text{Zn}(\text{CF}_3\text{SO}_3)_2$  without DA, significant pulverization and corrosion of the Zn electrode could be observed after long-term cycling.

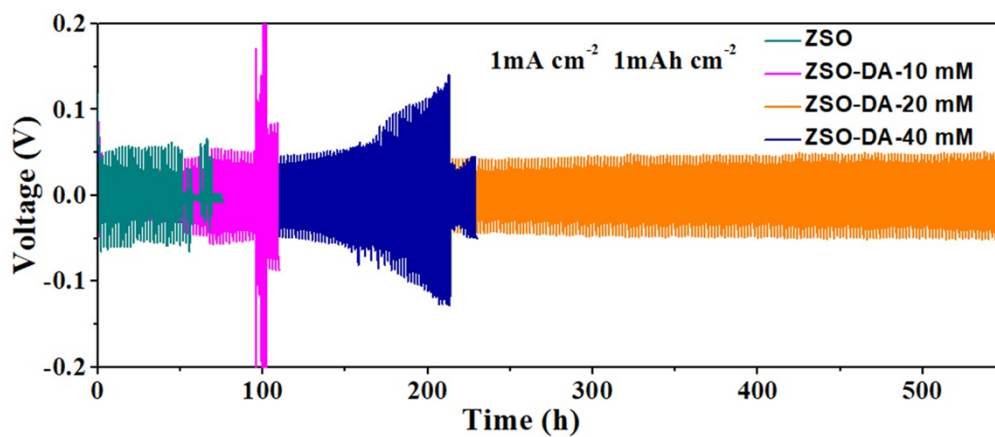


**Fig. S18** Comparison of galvanostatic cycling properties of Zn symmetrical cells in 1 M ZnSO<sub>4</sub> with 0, 10, 20, and 40 mM DA. The electrolyte consisting of 1 M ZnSO<sub>4</sub> with 20 mM DA exhibited optimal cycling stability.

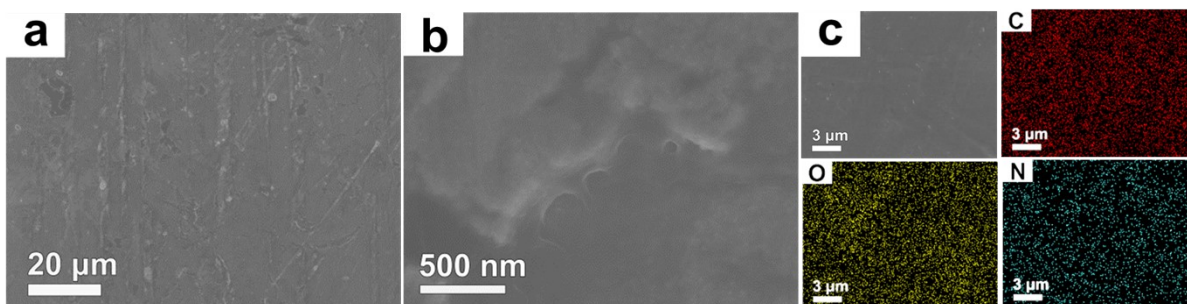


**Fig. S19** (a, b) SEM images and (c) corresponding EDX mapping of Zn electrodes after cycling in 1 M ZnSO<sub>4</sub> electrolyte with 20 mM DA. The SEM images of the cycled Zn display a smooth morphology without dendrites, and the EDX mapping indicates uniform distributions of C, N, and O on the Zn surface.

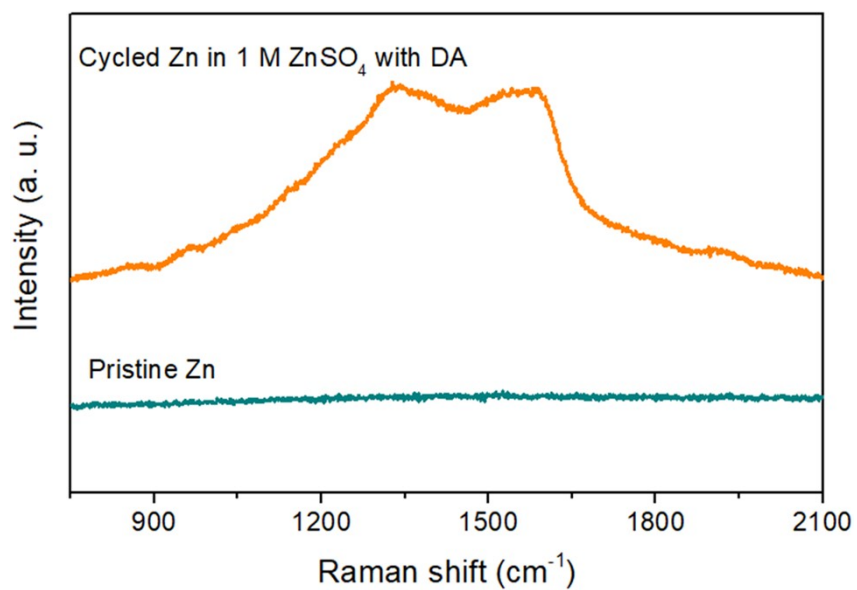


**Fig. S20** Raman spectra of pristine Zn and cycled Zn in 1 M ZnSO<sub>4</sub> with DA. The cycled Zn electrode in 1 M ZnSO<sub>4</sub> with DA was stripped out of its symmetrical cell (1 mA cm<sup>-2</sup>, 1 mA h cm<sup>-2</sup>) after 10 cycles. The emergence of the two broad peaks of the cycled Zn correspond to the stretching and deformation of aromatic rings of PDA.

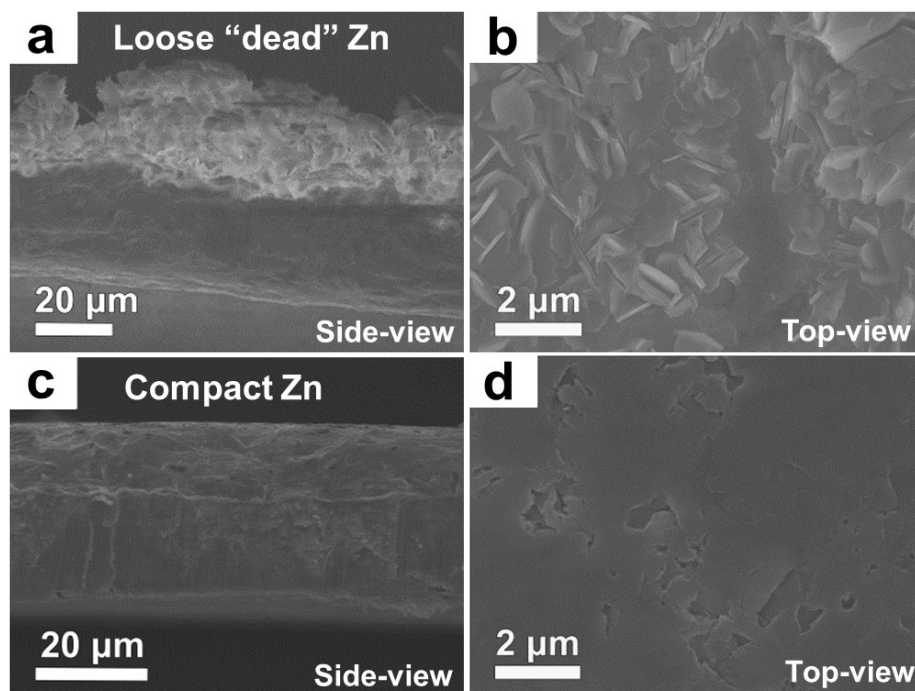


**Fig. S21** Side-view and top-view SEM images of Zn electrodes after cycling for 100 h in (a, b) 1 M ZnSO<sub>4</sub> without DA and (c, d) 1 M ZnSO<sub>4</sub> with 20 mM DA. The cycled Zn electrode in the blank electrolyte displayed loose and dendritic morphology, whereas a compact and smooth Zn electrode was obtained after cycling in the electrolyte with DA.

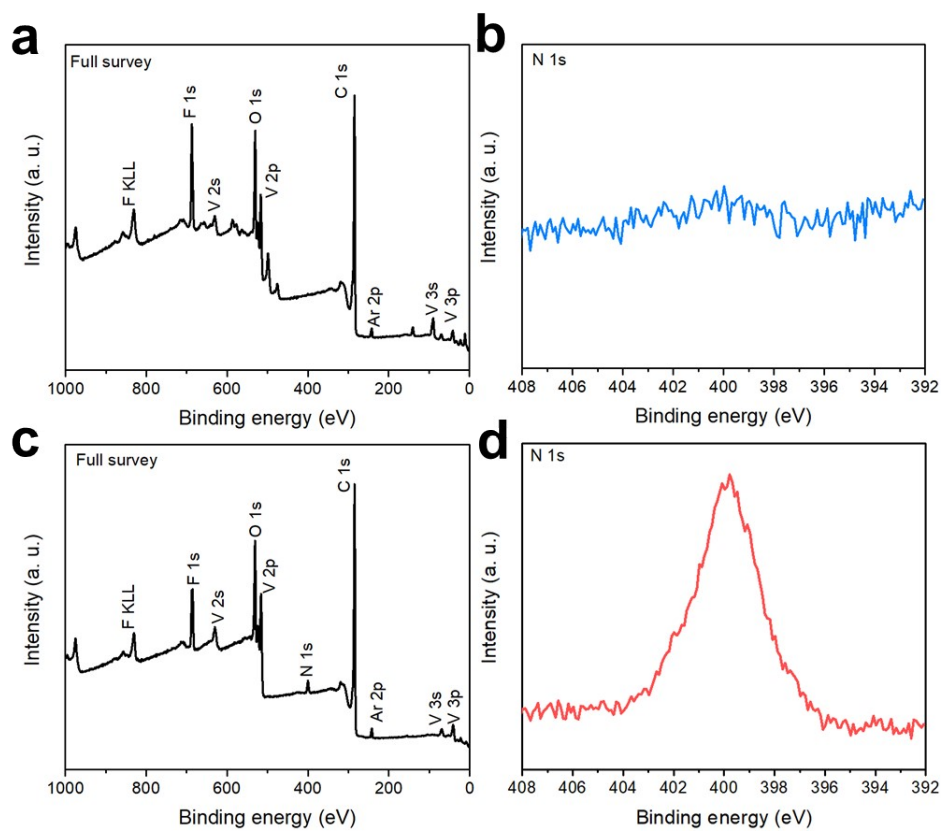


**Fig. S22** XPS characterization of  $V_2O_5$  cathode after cycling. (a, b) 1 M  $Zn(CF_3SO_3)_2$ , (c, d) 1 M  $Zn(CF_3SO_3)_2$  with DA additive as electrolyte.

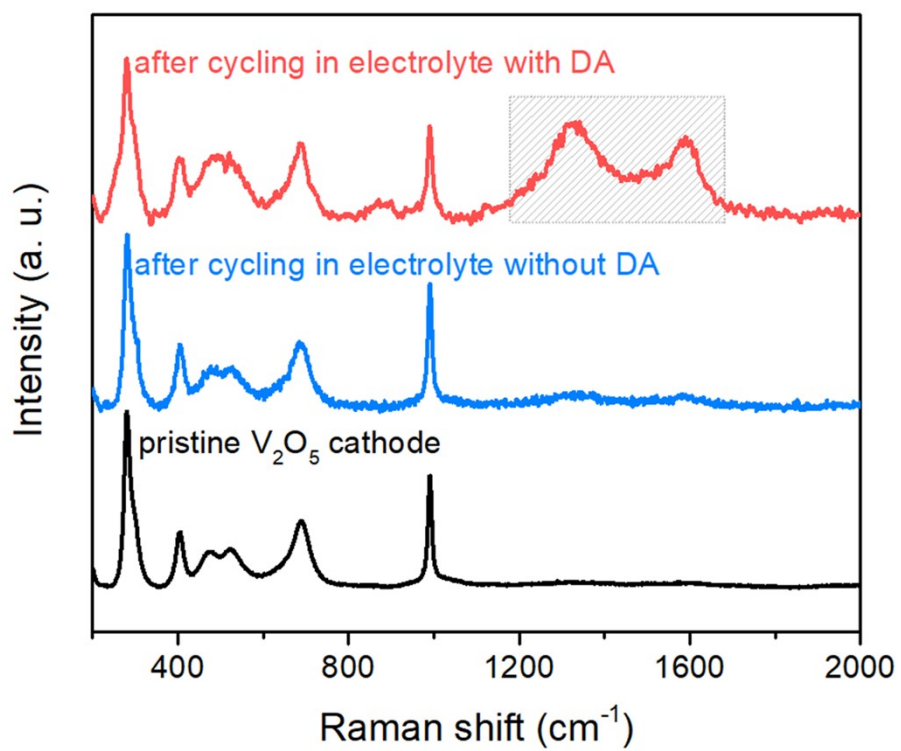
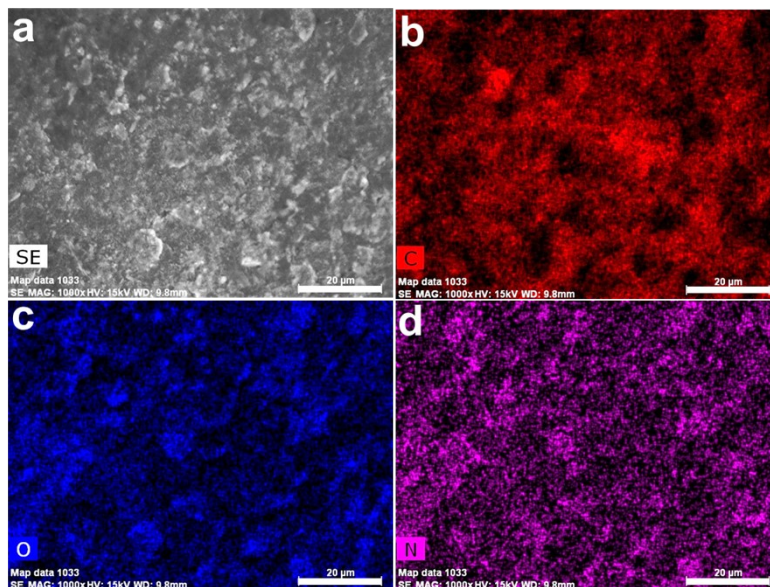
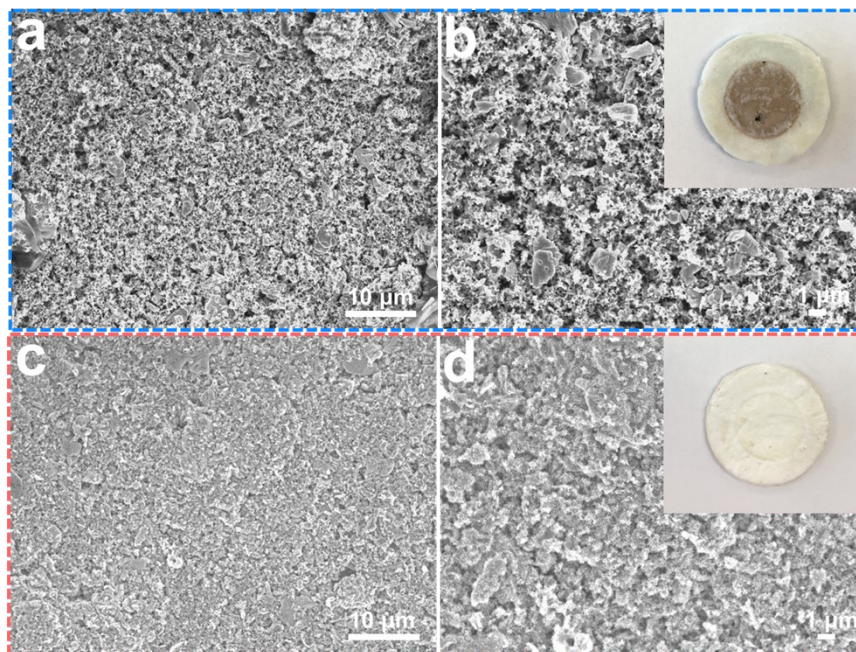


Fig. S23 Raman spectra of  $V_2O_5$  cathode before and after cycling.



**Fig. S24** (a) SEM image and (b-d) corresponding EDX mapping of V<sub>2</sub>O<sub>5</sub> cathode after the 10<sup>th</sup> cycle in 1 M Zn(CF<sub>3</sub>SO<sub>3</sub>)<sub>2</sub> with DA.



**Fig. S25** SEM images of cycled V<sub>2</sub>O<sub>5</sub> cathodes and digital images of glass fiber separators (insets) stripped from Zn/V<sub>2</sub>O<sub>5</sub> full cells after cycling at 1 A g<sup>-1</sup> for 200 cycles. (a, b) Cycling in 1 M Zn(CF<sub>3</sub>SO<sub>3</sub>)<sub>2</sub> electrolyte. (c, d) Cycling in 1 M Zn(CF<sub>3</sub>SO<sub>3</sub>)<sub>2</sub> electrolyte with 50 mM DA.

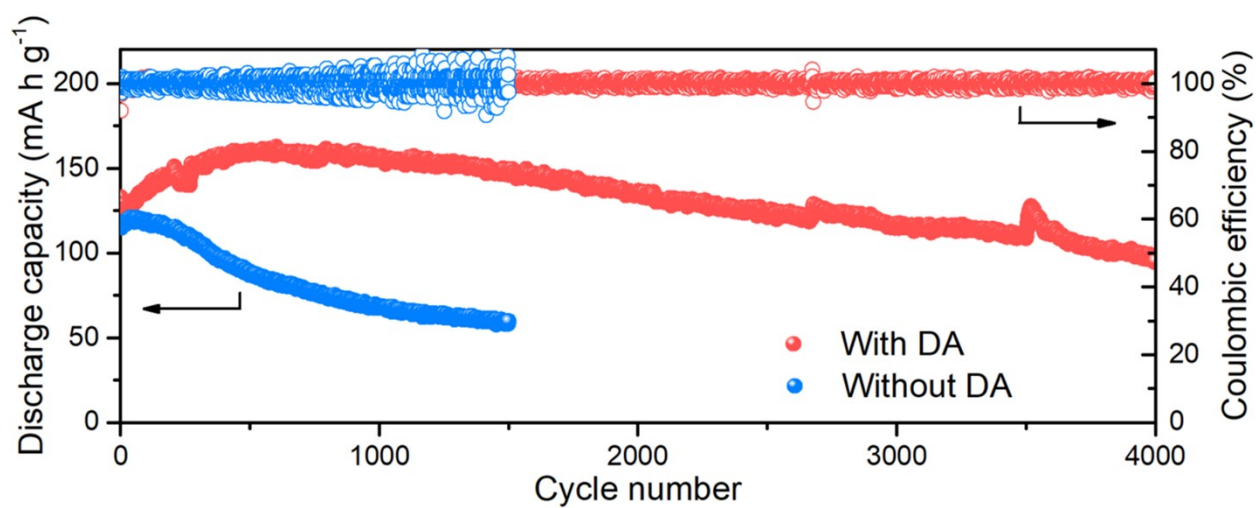


**Fig. S26** Long-term cycling stability of Zn/V<sub>2</sub>O<sub>5</sub> full cells with high excess Zn (thickness 60  $\mu\text{m}$ ) and electrolyte with and without DA. The applied current density was 1 A g<sup>-1</sup>.

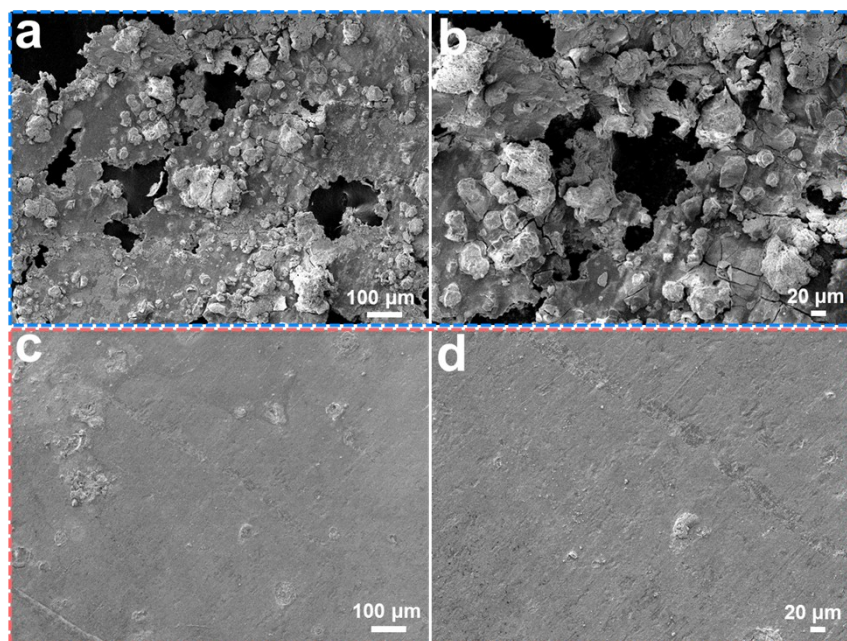


**Fig. S27** SEM images of ultrathin Zn electrodes (10  $\mu\text{m}$ ) after cycling for 200 cycles in Zn/V<sub>2</sub>O<sub>5</sub> full cells. (a, b) Cycling in 1 M Zn(CF<sub>3</sub>SO<sub>3</sub>)<sub>2</sub> as electrolyte, (c, d) cycling in 1 M Zn(CF<sub>3</sub>SO<sub>3</sub>)<sub>2</sub> with 50 mM DA.

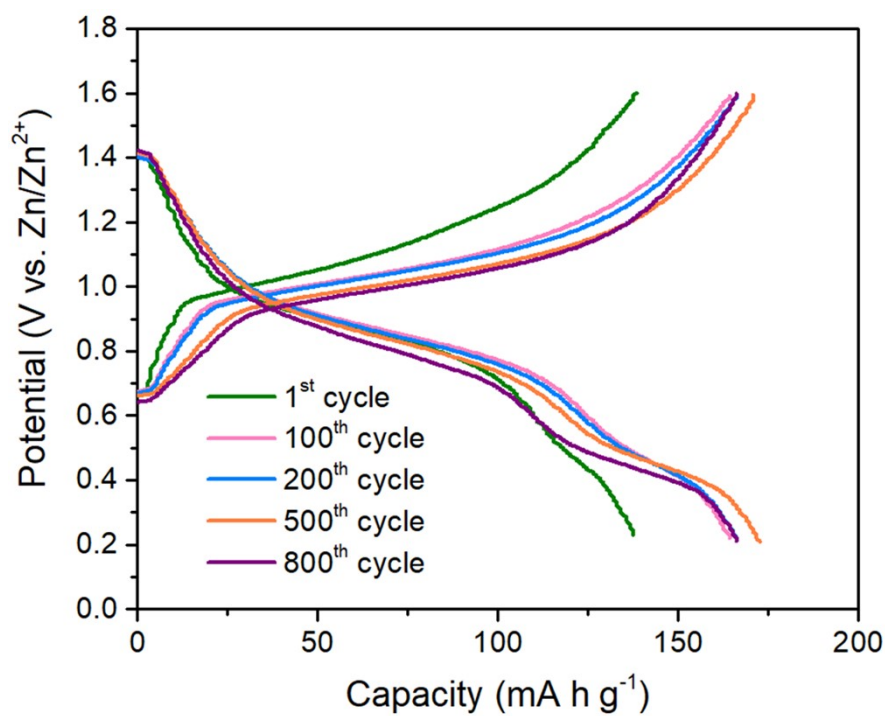


**Fig. S28** Charge/discharge curves of the Zn/V<sub>2</sub>O<sub>5</sub> full cell at 1 A g<sup>-1</sup>. The Zn/V<sub>2</sub>O<sub>5</sub> cell was tested at a current density of 1 A g<sup>-1</sup> in the electrolyte with DA additive. The electrolyte-to-capacity ratio (E/C) was controlled at 9 μL mAh<sup>-1</sup>, and the capacity ratio of the negative electrode to the positive electrode (N/P) was set to about 2.

**Table S1** Comparison of the electrochemical stability of state-of-the-art Zn metal electrodes at high current densities and areal capacities.

Electrode	Current density and areal capacity	Lifespan	Reference
<i>In situ</i> PDA-Zn	10 mA cm <sup>-2</sup> , 10 mA h cm <sup>-2</sup> 20 mA cm <sup>-2</sup> , 20 mA h cm <sup>-2</sup> 30 mA cm <sup>-2</sup> , 30 mA h cm <sup>-2</sup>	200 h 120 h 78 h	This work
Interdigitated Zn/IHS	20 mA cm <sup>-2</sup> , 20 mA h cm <sup>-2</sup>	80 h	<i>J. Am. Chem. Soc.</i> 2021, 143, 3143-3152
Zn/CNT	5 mA cm <sup>-2</sup> , 2.5 mA h cm <sup>-2</sup> 2 mA cm <sup>-2</sup> , 2 mA h cm <sup>-2</sup>	110 h 200 h	<i>Adv. Mater.</i> 2019, 31, 1903675
PA-coated Zn	10 mA cm <sup>-2</sup> , 10 mA h cm <sup>-2</sup>	75 h	<i>Energy Environ. Sci.</i> 2019, 12, 1938-1949
Zn in Zn(OTF) <sub>2</sub> -Zn(NO <sub>3</sub> ) <sub>2</sub>	10 mA cm <sup>-2</sup> , 10 mA h cm <sup>-2</sup>	90 h	<i>Angew. Chem. Int. Ed.</i> 2021, 60, 13035-13041
Zn(002)	10 mA cm <sup>-2</sup> , 2 mA h cm <sup>-2</sup>	200 h	<i>Angew. Chem.</i> 2021, 133, 7289-7295
Zn@ZnO HPA	5 mA cm <sup>-2</sup> , 2.5 mA h cm <sup>-2</sup>	100 h	<i>Adv. Funct. Mater.</i> 2020, 30, 2004210
CM@CuO@Zn	2 mA cm <sup>-2</sup> , 2 mA h cm <sup>-2</sup>	200 h	<i>Small</i> 2020, 16, 2000929
Zn@C	10 mA cm <sup>-2</sup> , 1 mA h cm <sup>-2</sup>	100 h	<i>ACS Appl. Mater. Interfaces</i> 2018, 10, 22059-22066
3D-Zn in TBA electrolyte	5 mA cm <sup>-2</sup> , 5 mA h cm <sup>-2</sup>	160 h	<i>ACS Energy Lett.</i> 2020, 5, 3012-3020
DCP-Zn-30	5 mA cm <sup>-2</sup> , 10 mA h cm <sup>-2</sup>	200 h	<i>Energy Storage Mater.</i> 2020, 30, 104-112
Zn in ZnSO <sub>4</sub> + LiCl	5 mA cm <sup>-2</sup> , 1 mA h cm <sup>-2</sup>	170 h	<i>ACS Energy Lett.</i> 2021, 6, 395-403
CaCO <sub>3</sub> -coated Zn	3 mA cm <sup>-2</sup> , 0.1 mA h cm <sup>-2</sup>	80 h	<i>Adv. Energy Mater.</i> 2018, 8, 1801090
Zn foam in 1 M ZnSO <sub>4</sub> + 1 M MnSO <sub>4</sub> + 0.1 M H <sub>2</sub> SO <sub>4</sub>	20 mA cm <sup>-2</sup> , 2 mA h cm <sup>-2</sup>	100 h	<i>Angew. Chem. Int. Ed.</i> 2019, 58, 7823-7828
Zn/SS mesh	2 mA cm <sup>-2</sup> , 1 mA h cm <sup>-2</sup>	300 h	<i>Nano Energy</i> 2019, 62, 94-102
Zn with 3D VG	5 mA cm <sup>-2</sup> , 5 mA h cm <sup>-2</sup>	75 h	<i>Adv. Mater.</i> 2020, 2003425
Zn@F-TiO <sub>2</sub>	2 mA cm <sup>-2</sup> , 2 mA h cm <sup>-2</sup>	280 h	<i>Nat. Commun.</i> 2019, 11, 3961

<b>Sc<sub>2</sub>O<sub>3</sub>-coated Zn</b>	2 mA cm <sup>-2</sup> , 2 mA h cm <sup>-2</sup>	240 h	<i>J. Energy Chem.</i> 2021, 55, 549-556
<b>Alg-Zn</b>	8.8 mA cm <sup>-2</sup> , 2.2 mA h cm <sup>-2</sup>	200 h	<i>Energy Storage Mater.</i> 2020, 27, 109-116
<b>Zn in PAM added electrolyte</b>	20 mA cm <sup>-2</sup> , 1 mA h cm <sup>-2</sup>	105 h	<i>Angew. Chem. Int. Ed.</i> 2019, 58, 15841-15847
<b>MOF-PVDF coated Zn</b>	3 mA cm <sup>-2</sup> , 3 mA h cm <sup>-2</sup>	100 h	<i>ACS Appl. Mater. Interfaces</i> 2019, 11, 32046-32051
<b>Zn/CNT foam</b>	3 mA cm <sup>-2</sup> , 0.5 mA h cm <sup>-2</sup>	167 h	<i>J. Mater. Chem. A</i> , 2020, 8, 11719-11727
<b>Cu foam @Zn</b>	2 mA cm <sup>-2</sup> , 1 mA h cm <sup>-2</sup>	150 h	<i>Chem. Eng. J.</i> 2020, 379, 1222482

## References

1. G. Kresse and J. Furthmüller, *Comput. Mater. Sci.*, 1996, **6**, 15-50.
2. P. E. Blöchl, *Phys. Rev. B*, 1994, **50**, 17953.
3. J. P. Perdew, J. A. Chevary, S. H. Vosko, K. A. Jackson, M. R. Pederson, D. J. Singh and C. Fiolhais, *Phys. Rev. B*, 1992, **46**, 6671.
4. S. Grimme, J. Antony, S. Ehrlich and H. Krieg, *J. Chem. Phys.*, 2010, **132**, 154104.
5. G. Henkelman, B. P. Uberuaga and H. Jónsson, *J. Chem. Phys.*, 2000, **113**, 9901–9904.